ROYAL SOCIETY
OF CHEMISTRY

PAPER

Check for updates

Modification of cellulose through physisorption of cationic bio-based nanolatexes – comparing emulsion polymerization and RAFT-mediated polymerization-induced self-assembly†

Alexandros E. Alexakis, [a,b] Joakim Engström, [a,b] Arne Stamm, [a]
Anastasia V. Riazanova, [b] Calvin J. Brett, [a,b,c] Stephan V. Roth, [a,c]
Per-Olof Syrén, [a,b] Linda Fogelström, [a,b] Michael S. Reid [d] and
Eva Malmström *[a,b]

The polymerization of a bio-based terpene-derived monomer, sobrerol methacrylate (SobMA), was evaluated in the design of polymeric nanoparticles (nanolatexes). Their synthesis was accomplished by using emulsion polymerization, either by free-radical polymerization in the presence of a cationic surfactant or a cationic macroRAFT agent by employing RAFT-mediated polymerization-induced self-assembly (PISA). By tuning the length of the hydrophobic polymer, it was possible to control the nanoparticle size between 70 and 110 nm. The average size of the latexes in both wet and dry state were investigated by microscopy imaging and dynamic light scattering (DLS). Additionally, SobMA was successfully copolymerized with butyl methacrylate (BMA) targeting soft-core nanolatexes. The comparison of the kinetic profile of the cationically stabilized nanolatexes highlighted the differences of both processes. The SobMA-based nanolatexes yielded high $T_g \sim 120$ °C, while the copolymer sample exhibited a lower $T_g \sim 50$ °C, as assessed by Differential Scanning Calorimetry (DSC). Thereafter, the nanolatexes were adsorbed onto cellulose (filter paper), where they were annealed at elevated temperatures to result in polymeric coatings. Their morphologies were analysed by Field Emission Scanning Electron Microscopy (FE-SEM) and compared to a commercial sulfate polystyrene latex (PS latex). By microscopic investigation the film formation mechanism could be unravelled. Water contact angle (CA) measurements verified the transition from a hydrophilic to a hydrophobic surface after film formation had occured. The obtained results are promising for the toolbox of bio−based building blocks, focused on sobrerol-based monomers, to be used in emulsion polymerizations either for tailored PISA−latexes or facile conventional latex formation, in order to replace methyl methacrylate or other high T_g-monomers.

Introduction

(Meth)acrylate monomers are widely used, particularly in coating and adhesive applications.[1] Their respective macro-molecules are prepared mainly by free radical polymerization techniques from fossil-based building blocks.[2,3] However, there are bio-based alternatives that can replace fossil-based monomers, but there are problems concerning upscaling their production.[4] Therefore, it is of significant interest to increase the availability of bio-based monomers, especially in water-borne systems. A special interest has been devoted to wood-based sources, due to its large abundance.[5] In this context, turpentine, a pine-tree resin, is comprised primarily from α-pinene.[6] The high annual production of turpentine, which exceeds 300 000 tons, makes it a promising bio-based sub-strate.[7] Furthermore, through the transformation of α-pinene, a new diol is derived, sobrerol.[8] Sobrerol is a cyclic, high temperature profile monomer, which possesses a secondary hydroxyl group that is more reactive than the tertiary and its six-member ring carries a double bond. Its multifunctionality

[a]KTH Royal Institute of Technology, School of Engineering Sciences in Chemistry, Biotechnology and Health, Department of Fibre and Polymer Technology, Division of Coating Technology, Teknikringen 56-58, SE-100 44 Stockholm, Sweden. E-mail: mavem@kth.se
[b]Wallenberg Wood Science Centre (WWSC), Teknikringen 56-58, SE-100 44 Stockholm, Sweden
[c]Deutsches Elektronen-Synchrotron (DESY), Notkestrasse 85, 22603 Hamburg, Germany
[d]KTH Royal Institute of Technology, School of Engineering Sciences, Department of Engineering Mechanics, Osquarsbacke 18, SE-100 44 Stockholm, Sweden
†Electronic supplementary information (ESI) available. See DOI: 10.1039/d0gc04266h

equips sobrerol with interesting properties and possibilities for orthogonal chemistry. Sobrerol can be readily methacrylated to form SobMA (Fig. 1)[8,9] and has been shown that it can be polymerized by controlled radical polymerization (CRP) techniques such as both reversible addition–fragmentation chain-transfer (RAFT) and atom transfer radical polymerization (ATRP).[9]

The production of colloidal polymer particles in aqueous media, latexes, has primarily relied on oil-based (meth)acrylates and styrenics using low molecular weight stabilizers. However, this approach faces challenges, such as the scarcity of bio-based alternatives and the tailoring of particle dimensions and charge on-demand.[3,10–17] The use of CRP techniques, such as RAFT polymerization, provides a versatile possibility on tailoring the synthesis technique in order to bypass the use of surfactants.[13,18,19] A prerequisite is the use of chain-extension of a macromolecule called macroRAFT agent by hydrophobic monomers in water, leading to the formation of a stable latex. This process is called polymerization-induced self-assembly (PISA) and it has been demonstrated that the applied macroRAFT agent could possess different functionalities and thus tailor the surface properties of the formed latexes.[20–23] For instance, it could be hydrophilic by using a carbohydrate such as xyloglucan[24] or zwitterionic by using an amino acid such as cysteine.[25] The choice of the macroRAFT is based on the final application of the produced latexes. For example, when targeting anionic cellulose surfaces, the use of cationic polymers 2-(dimethylamino)ethyl methacrylate (PDMAEMA) and N-[3-(dimethylamino)propyl]methacrylamide (PDMAPMA) has shown interesting properties. Specifically, they not only have been shown

to preserve the control of the polymerization, but also to allow for efficient tailoring of particle size and charge density.[26–28] The necessity to modify cellulose is primarily derived from its incompatibility in composite applications due to its hydrophilic nature. Hence, the modification of its surface properties is of utmost importance. Within this context, filter papers, being a facile cellulose substrate, have been coated with the aforementioned nanolatexes in order to alter their surface hydrophilicity. In detail, latexes of which the corona is comprised of PDMAEMA[27] or xyloglucan[24] were successfully adsorbed on filter paper in order to convert the substrate to a hydrophobic surface.

Notwithstanding the previous work on SobMA polymerizations, this study aims to utilize SobMA in emulsion polymerization using only water and no organic solvents, which according to the best of the authors' knowledge has never been performed. For this reason, SobMA is homo- and copolymerized with butyl methacrylate (BMA), resulting in high and low glass transition temperature nanolatexes, respectively, the adhesion of which is investigated on cellulose surfaces. To widely explore the use of SobMA, conventional latexes using low molecular weight cationic surfactant (cetyltrimethylammonium chloride (CTAC)) and P(DMAEMA-co-MAA) macroRAFT agent through RAFT-mediated surfactant-free emulsion polymerization with PISA are evaluated in parallel. The latter will also be reported for the first time, which expands the scope of the monomer and the use of the previously investigated macroRAFT agent, as well as its ability to successfully stabilize bio-based latexes. Additionally, PISA-based nanolatexes differ from the surfactant-based counterparts in terms of the length of the stabi-
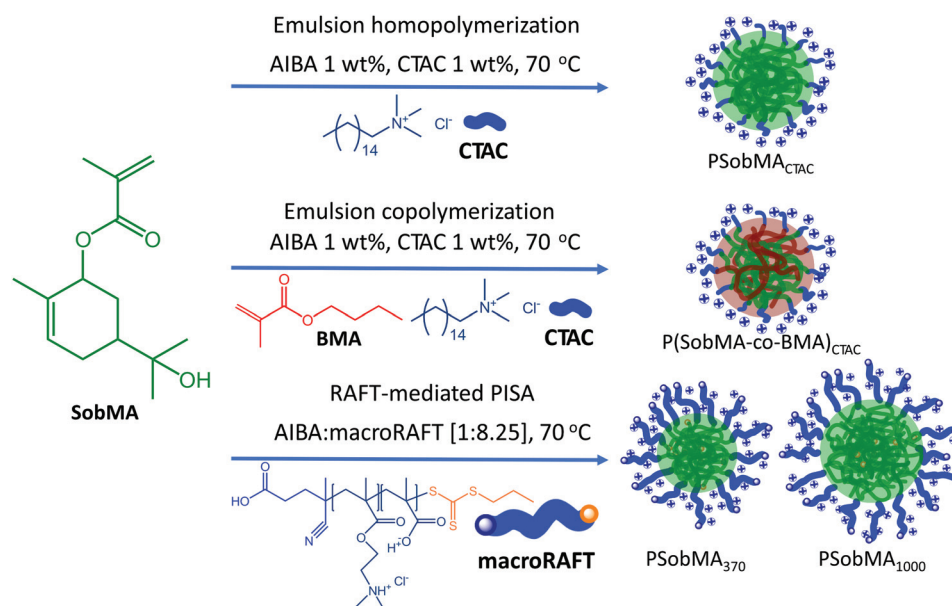

Fig. 1 Schematic representation of surfactant-based emulsion homopolymerization of SobMA (upper arrow), copolymerization of SobMA-co-BMA (middle arrow) and RAFT-mediated surfactant-free emulsion polymerization-induced self-assembly (PISA) (lower arrow) resulting in the formation of stable nanosized latexes.

lizing agent, which is expected to affect their film formation properties. The use of SobMA is motivated by its renewability, as it is derived from α-pinene; at the same time, it also brings functionality into the hydrophobic core of the latex, due to the tertiary hydroxyl group and the alkene present in every repeating unit.

The SobMA-containing latexes were characterized with respect to chemical composition (^{1}H-nuclear magnetic resonance (^{1}H-NMR)), molecular weight (size exclusion chromatography (SEC)), thermal properties (differential scanning calorimetry (DSC)), and their particle size/size distribution (dynamic light scattering (DLS), atomic force microscopy (AFM) imaging and field emission scanning electron microscopy (FE-SEM)). Based on the already published findings that P(DMAEMA-co-MAA)-stabilized PISA latexes are readily adsorbed to cellulose,[27,28] the latexes were also adsorbed onto cellulose (filter papers) and the resulting surfaces were analysed in terms of morphology and wetting (FE-SEM and contact angle (CA)).

Experimental

Materials

n-Butyl methacrylate (BMA, 99%), 2,2′-azobis(2-methylpropionamidine) dihydrochloride (AIBA, 97%), cetyltrimethylammonium chloride (CTAC, 25 wt% water solution) and (2-dimethylaminoethyl) methacrylate (DMAEMA, 98%) were all purchased from Sigma Aldrich and used as received. Dimethyl sulfoxide-d_6 (DMSO-d_6, 99.9%), chloroform-d (CDCl$_3$, 99.8%) and deuterium oxide (D$_2$O, 99.9%) were all purchased from VWR and used as received. Sulfate polystyrene latex (PS latex, 8% w/v, 0.2 μm) were purchased from Thermo Fischer Scientific. The hydrophobic monomer, sobrerol methacrylate (SobMA), was synthesized in analogy to previously published protocols either with the enzymatic or the typical methacrylation approach.[8,9] The water used was either deionized or Milli-Q water. RAFT agent 4-cyano-4-thiothiopropylsulfanyl pentanoic acid (CTPPA) was synthesized according to literature procedure.[29,30] Munktell cellulose filter paper grade 3 (Ahlstrom, Munktell) was used for adsorption of latexes.

Characterization techniques

Nuclear magnetic resonance (NMR). The polymerization of DMAEMA for the synthesis of the cationic macroRAFT was monitored by ^{1}H-NMR with a Bruker Avance AM 400 NMR instrument using D$_2$O as solvent. The degree of hydrolysis (D_H) of DMAEMA to methacrylic acid (MAA) (Fig. S1 and eqn (S1)†), was estimated in accordance to previously published work.[26] The weight fraction of SobMA in the residual solvents used during its purification, i.e. ethyl acetate and dichloromethane, was estimated by ^{1}H-NMR in CDCl$_3$ (Fig. S2†). The homo- and copolymerizations of SobMA with BMA were monitored by ^{1}H-NMR using DMSO-d_6 and CDCl$_3$ as solvent, respectively. For the estimation of conversion (p) of the

monomer, the methine proton peak at 5.2 ppm was used and compared with its respective broad peak around 5.0 ppm, which corresponds to the same proton when SobMA is polymerized (Fig. S3 and eqn (S2)†). All samples used for the ^{1}H-NMR were freeze-dried overnight prior to their characterization.

Size exclusion chromatography (SEC). SEC analysis of the polymers was performed on a TOSOH EcoSEC HLC-8320GPC system equipped with an EcoSEC RI detector and three columns (PSS PFG 5 μm; Microguard, 100 Å, and 300 Å; MW resolving range: 100–300 000 g mol^{-1}) from PSS GmbH, using DMF as solvent with 0.01 M LiBr as the mobile phase at 50 °C with a flow rate of 0.2 mL min^{-1}. A calibration method with PMMA standards was used ranging from 700 to 2000 000 g mol^{-1}. All samples were freeze dried prior to their characterization. The results of this analysis can be found in Table S2.†

Differential scanning calorimetry (DSC). DSC analysis was performed with a Mettler Toledo DSC. All nanolatexes were analysed with heating and cooling rate of 10 °C min^{-1} in nitrogen atmosphere. The method used comprised of two heating cycles and one cooling; heating from 25 to 170 °C, equilibrating for 5 min, then cooling from 170 to −60 °C, equilibrating for 5 min and finally a second heating ramp from −60 to 170 °C. Data from the second heating cycle were used to evaluate the glass transition temperature (T_g) for all samples. The nanolatexes were freeze-dried prior to analysis.

Dynamic light scattering (DLS). The hydrodynamic diameter (D_H), given as Z-average, polydispersity index (PdI) and electrophoretic mobility (ζ potential) of the nanolatexes were determined using a Malvern Zetasizer NanoZS at 25 °C. Each value used in this study is averaged over three samples (three different batches of samples, except from PSobMA$_{CTAC}$ which was two) from which, each one is obtained as an average of three consecutive runs (Table S3†). For all of the above measurements, the concentration of the latex dispersions was approximately 10 vol% and the solvent used was Milli-Q water. The standard used for the size correlation of the investigated latexes was polystyrene, set by default from the instrument.

Atomic force microscopy (AFM). AFM images were collected using a Multimode 8 in TappingMode with RTESP-150 (Bruker, CA, USA) cantilevers having a nominal spring constant of 5 N m^{-1} and a resonant frequency of 150 kHz. Samples were prepared by spin coating 0.1 wt% dispersions onto clean silica wafers. Images were processed using NanoScope Analysis v1.6 software. Particle diameter distributions were determined using Gwyddion v2.54 software.

Fourier transform infrared spectroscopy (FT-IR). The infrared spectra of latex modified and non-modified cellulose filter papers were recorded with a PerkinElmer Spectrum 2000 FTIR equipped with a MKII Golden Gate, single reflection ATR crystal with a MKII heated diamond 45° ATR top plate (from Specac Ltd, London, UK). All paper samples were analysed by 16 scans and normalized to the crystal region ranging between 2400 to 1900 cm^{-1}. The results of this analysis can be found in Fig. S8.†

Field emission scanning electron microscopy (FE-SEM). A Hitachi S-4800 FE-SEM was used for the characterisation of modified and non-modified cellulose filter papers as well as the morphology of nanolatexes which were spin coated on clean silica wafers (previously used in AFM). The voltage used was set at 1 kV for all images taken. Each sample was sputtered for 10 s resulting in 0.7 nm layer of Pt/Pd (Cressington sputter coater 208RH), except from the spin coated samples on silica wafers, which were not sputtered. The particle diameters of the spin coated samples were determined using Gwyddion v2.54 software.

Contact angle (CA). Water CA measurements were performed using a measurement setup OCA 35 (DataPhysics Instruments GmbH, Germany) and remote-controlled syringes (series 1750, Hamilton Germany GmbH, Germany). All samples were kept for 24 h at 30% RH at 25 °C. The sessile drop method with a volume of 5 μL water and a dispensing speed of 5 μL s^{-1} was used. The deposited droplet was captured by a camera using a shutter of 5 s after the droplet hit the surface. The resulting image was evaluated using the software SCA 20 (DataPhysics Instruments GmbH, Germany) to obtain the average CA. The baseline as well as the elliptical shape of the droplet was automatically retrieved from the program. Each droplet yields a CA value from the right and one from the left of the droplet which give the average CA of the sample. Each sample was measured on three distinct positions on both sides of the sample to increase the statistics and check the homogeneity. The pictures obtained from this method are found in Fig. S13.†

Synthetic procedures

Emulsion homo- and copolymerization of SobMA and SobMA-*co*-BMA latexes using CTAC. The latex system was produced by emulsion polymerization using CTAC as surfactant (Fig. 1, *upper arrow*). A typical protocol for the production of latexes (Table 1, sample PSobMA$_{CTAC}$) is as follows: SobMA (1.0 g of dry monomer, 4.2 mmol) was introduced in a 25 mL round bottom flask equipped with a magnetic stirring bar and put in the rotary evaporator to remove the stabilizing solvents. Then, CTAC (31.1 μmol, 3.42 mM, 1 wt% compared to SobMA) and an aqueous solution of the initiator AIBA (3.4 g L^{-1}) were added to the round bottom flask (36.8 μmol, 1 wt% compared to SobMA), followed by deionized water (6.2 mL) targeting 10 wt% of dry content (eqn (S3)†). The flask was placed in an ice/water bath and the reaction mixture was degassed with argon for 30 min and thereafter immersed into an oil bath pre-heated to 70 °C, thus initiating the polymerization. All reactions were performed for 120 min. The same protocol was followed for the copolymerization of SobMA with BMA (Fig. 1, middle arrow). In this case, the calculations were based on having the same concentration of CTAC in the system as in the homopolymerization (Table 1, sample P(SobMA-*co*-BMA)$_{CTAC}$). BMA comprised 85 wt% of total monomer content, whereas CTAC and AIBA were set to 1 wt% of total monomer content. The content of BMA was chosen as such to target latexes with T_g closer to room temperature. Aliquots were taken during both polymerizations, which were analysed by DLS, AFM and FE-SEM and finally freeze dried and analysed using ^{1}H-NMR, SEC and DSC. The values of each reagent used for each sample are listed in Table S1.†

RAFT-mediated PISA of SobMA latexes. The novel synthesis of PSobMA latexes was conducted by employing a pre-formed P(DMAEMA-*co*-MAA) macroRAFT synthesized in water which had an experimentally determined molecular weight (M_n) around 4100 g mol^{-1}.[27] The DMAEMA is hydrolysed into MAA during synthesis (D_H 2.9%), hence the copolymer (Fig. S1†).[26] The macroRAFT is chain-extended with SobMA in water, resulting in the formation of PISA-latexes as shown schematically in Fig. 1, lower arrow. In a typical experiment (Table 1, sample PSobMA$_{370}$), SobMA (1.1 g of dry monomer, 4.6 mmol, target DP 370) was added in a 25 mL round bottom flask equipped with a magnetic stirring bar and the aforementioned solvents were evaporated. Thereafter, the macroRAFT agent (516.7 mg, 12.5 μmol) was added followed by the addition of an aqueous solution of the initiator AIBA (3.4 g L^{-1}) (1.5 μmol in 1 : 8.25 molar ratio to the macroRAFT). Deionized water was added (10.3 mL) to reach a final dry content of 10 wt% and the flask was immersed in an ice/water bath and degassed with argon for 30 min. Finally, it was immersed into an oil bath which was pre-heated to 70 °C, which is the time zero for the polymerization. All reactions were performed for 120 min.

Table 1 The physicochemical properties of the different nanolatexes of SobMA and SobMA-*co*-BMA produced for this study through surfactant-based and surfactant-free emulsion polymerization

Materials	p^d (%)	D_{AFM}^e (nm)	D_{SEM}^f (nm)	D_H^g (nm)	PdI^g	Z^g (mV)	$N_P 10^{14\,h}$(mL^{-1})	T_g^i (°C)
PSobMA$_{CTAC}$^{a}	91	76 ± 24	78 ± 23	109 ± 1	0.09 ± 0.01	51 ± 4	1.21 ± 0.02	123 ± 2
P(SobMA-*co*-BMA)$_{CTAC}$^{a}	98	81 ± 20	93 ± 28	110 ± 3	0.03 ± 0.01	49 ± 4	1.31 ± 0.10	50 ± 2
PSobMA$_{370}$^{b}	83	38 ± 17	52 ± 16	73 ± 1	0.08 ± 0.01	53 ± 2	3.94 ± 0.55	119 ± 7
PSobMA$_{1000}$^{b}	83	58 ± 28	73 ± 23	112 ± 17	0.09 ± 0.03	54 ± 10	1.13 ± 0.55	127 ± 11
PS latex^c	—^{j}	—^{j}	—^{j}	215 ± 1	0.03 ± 0.02	−40 ± 1	0.150 ± 0.002	104 ± 1

^{a} Synthesized using CTAC as surfactant and AIBA as initiator targeting 10 wt% dry content. ^{b} Synthesized using macroRAFT as stabilizer and AIBA as initiator targeting 10 wt% dry content. The target DP is shown in subscript. ^{c} Commercial sulfate polystyrene latex. ^{d} Total monomer conversion (p) calculated from ^{1}H-NMR in DMSO-d_6 and CDCl$_3$ (eqn (S2)). ^{e} Measured by AFM on spin coated silica wafers with 0.1 wt% of latex dispersion. ^{f} Measured by FE-SEM on the same samples used for AFM. ^{g} Measured from DLS with 10 vol% dispersion in MilliQ water. The DLS values (D_H, PdI and ζ) are the average of three samples (Table S3†). ^{h} Obtained from eqn (S6) by using D_H. ^{i} Obtained from the second heating run of DSC measurement and averaged over three samples. ^{j} Not applicable.

Aliquots were taken during polymerization and analysed with DLS, AFM and FE-SEM and thereafter freeze dried and characterized using ^{1}H-NMR, SEC and DSC. The amounts of the reagents are listed in Table S1.†

The latexes synthesized with CTAC were abbreviated PSobMA$_{CTAC}$ (homopolymerization of SobMA) and P(SobMA-co-BMA)$_{CTAC}$ (copolymerization of SobMA with BMA), whereas PISA-latexes were abbreviated with the core polymer and target DP in subscript, i.e. PSobMA$_{370}$ and PSobMA$_{1000}$.

Adsorption of latexes onto cellulose (filter paper) substrate. The nanolatexes were adsorbed onto cellulose filter paper pieces (1×1 cm^2). They were initially soaked with deionized water and then immersed in different vials containing the synthesized nanolatexes with an average dry content of 1 wt%. The filter paper pieces were left in the vial on a stirring table for 24 h to ensure complete adsorption. Thereafter, they were thoroughly rinsed with deionized water and they were divided into three batches depending on the drying conditions. The first batch was left to dry in a conditioning room at 23 °C and 50% RH overnight. The second and the third were put in an oven operating at 150 °C for 1 h and 8 h, respectively, and thereafter stored in the same conditioning room as above. The samples were characterized by FTIR, FE-SEM and CA. Filter paper with no adsorbed latexes was also subjected to the same heating and storing conditions and analysed with the same techniques for reference purposes.

Results and discussion

Kinetic results of cationic nanolatexes

Striving towards renewable monomers for radical polymerization, the methacrylation of sobrerol, to produce sobrerol methacrylate (SobMA) was accomplished in accordance to previously published protocols.[8,9] In this work, SobMA is being investigated in waterborne systems and specifically in emulsion polymerizations with and without surfactant in order to expand its versatility.

The results are divided into three parts. In the first part, the kinetic profiles of the surfactant-based and surfactant-free emulsion homo- and copolymerizations of SobMA and butyl methacrylate (BMA) are discussed in detail. Also, in this part, the two different approaches are compared. In the second part, the final morphological and thermal properties of latexes originating from both approaches are investigated. In both parts, analyses of the polymeric constituents and their particle properties in the wet state, being nanosized colloids, are discussed. The third part focuses on the film formation ability of latexes as well as their dry state particle structures when adsorbed onto cellulose (filter paper) surfaces.

Initially, SobMA was either successfully homo- or copolymerized with BMA in water using a commercial cationic surfactant, cetyltrimethylammonium chloride (CTAC) (Fig. 1, upper and middle arrows, respectively). Additionally, a cationic macroRAFT agent was chain extended with SobMA in water with RAFT-mediated surfactant-free emulsion polymerization

during polymerization-induced self-assembly (PISA) (Fig. 1, lower arrow). In both approaches, the polymerization was initiated by the cationic azo-initiator 2,2′-azobis(2-methylpropionamidine) dihydrochloride (AIBA) and the resulting latex properties are summarized in Table 1. Throughout, sample names are abbreviated with respect to their nanoparticle's core monomer and in subscript either the stabilizer CTAC (e.g. PSobMA$_{CTAC}$) for surfactant-based, or the target degree of polymerization (DP) (e.g. PSobMA$_{370}$) for the surfactant-free latexes, respectively.

The synthesis and the colloidal stability of the polymerization can primarily be evaluated from three aspects: the kinetics of the polymerization, the size and control of the resulting polymer stabilized latexes and the resulting block copolymer formation in the case of PISA-latexes (RAFT-mediated synthesis to be the cause of self-assembly). The reproducibility of all polymerizations was evaluated by producing triplicate latex batches (except for PSobMA$_{CTAC}$ where only two batches were used) (Table S3†).

Usually, kinetics is monitored by the gravimetry, which rely on the fact that the monomer/s used is/are volatile and thus evaporate/s. However, that is not the case for SobMA. It is reported that SobMA has a high boiling point and is therefore difficult to evaporate without causing autopolymerization.[9] Hence, a more accurate way to follow the polymerization kinetics is by ^{1}H-NMR. The conversion was calculated by comparing the methine proton next to the methacrylate peak while in the monomer (5.2 ppm) and polymer configuration (broad peak around 5.0 ppm) (Fig. S3†). Additionally, the double bond of the six-membered-ring of SobMA remained unaffected by the polymerization as suggested by ^{1}H-NMR (Fig. S5†). The kinetic data suggest that surfactant-based latexes polymerize more rapidly compared with PISA-latexes. Furthermore, only the PISA-systems exhibit inhibition periods of approximately 15 min (Fig. 2). Inhibition periods are frequently observed in PISA-systems when the kinetics is monitored by ^{1}H-NMR[31,32] or gravimetry.[27] Additionally, in Fig. 2 it is shown that the surfactant-based systems reach higher conversions at shorter reaction times compared to the PISA-based. Specifically, the plateau is reached after approximately 45 min, corresponding to 90% of conversion and 75 min corresponding to 83% of conversion for surfactant and PISA-based systems, respectively (Table 1). One of the reasons why neither of the systems reach full conversion may be the fact that air could have been introduced in the reaction flask when aliquots were taken for analysis during the polymerization. Additionally, SEC results showed high deviations between the theoretical and experimental molecular weight obtained (Table S2†). This can be attributed to different reasons. Firstly, SEC is a relative technique where the investigated diblock copolymer samples are compared to conventional homopolymer (PMMA calibration standard). Secondly, similarly charged nanolatexes have shown inaccurate estimation of the molecular weight in the literature.[27] Finally, although the discrepancy is high, increasing the target DP of the core resulted in increasing molecular weight.
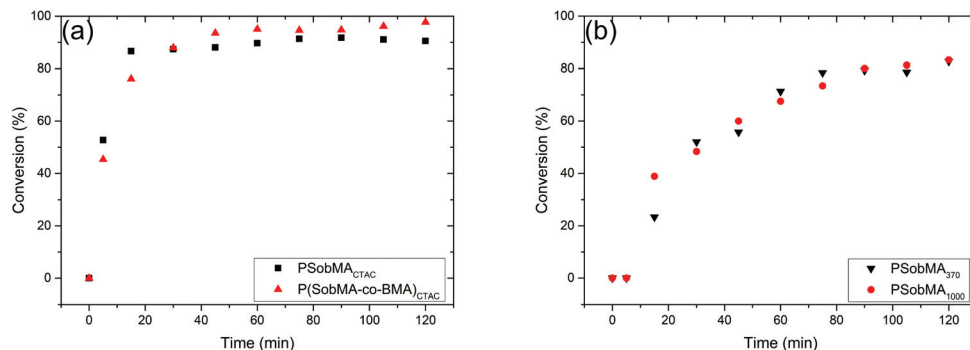
Fig. 2 Conversion plots of the nanolatexes prepared with surfactant-based emulsion polymerization (a) and surfactant-free RAFT-mediated emulsion polymerization-induced self-assembly (PISA) (b). The samples depicted in the graphs are shown in the inlet label.

The aforementioned observations based on the kinetic profile of the samples are further strengthened by monitoring the evolution of particles size by DLS (Fig. 3). In the beginning, the emulsion polymerization is characterized by the presence of monomer droplets and surfactant. For all samples, the formation of latexes is characterized by a sharp decrease in the monitored size. For PISA synthesized latexes, this decrease signals that the critical chain length of the hydrophobic block has been achieved, meaning that the block copolymer starts to self-assemble into a latex (Fig. 3c and d).[20] Afterwards, the formed latex nanoparticles start to grow by diffusion of monomer to their core, which is translated into an increase of the particle size. It is observed that

this diffusion takes longer time for PISA-systems than surfactant-based systems, which can be correlated to the faster monomer consumptions (Fig. 2). Finally, the latexes obtain their final size which is indicated by the plateau observed in both particles' size (Fig. 3) and number of particles (N_p) (Fig. S6†). As mentioned previously, the final size of the latex nanoparticle is achieved earlier for surfactant-based latexes (Fig. 2a). However, it is worth noting that P(SobMA-*co*-BMA)$_{CTAC}$ exhibits a slight increase in size at higher reaction times, where the final diameter recoded is similar to that of PSobMA$_{CTAC}$, being 110 and 109 nm, respectively (Table 1). Furthermore, the polydispersity index (*PdI*) obtained from DLS (Fig. S4†) verified the equilibrium which is reached at
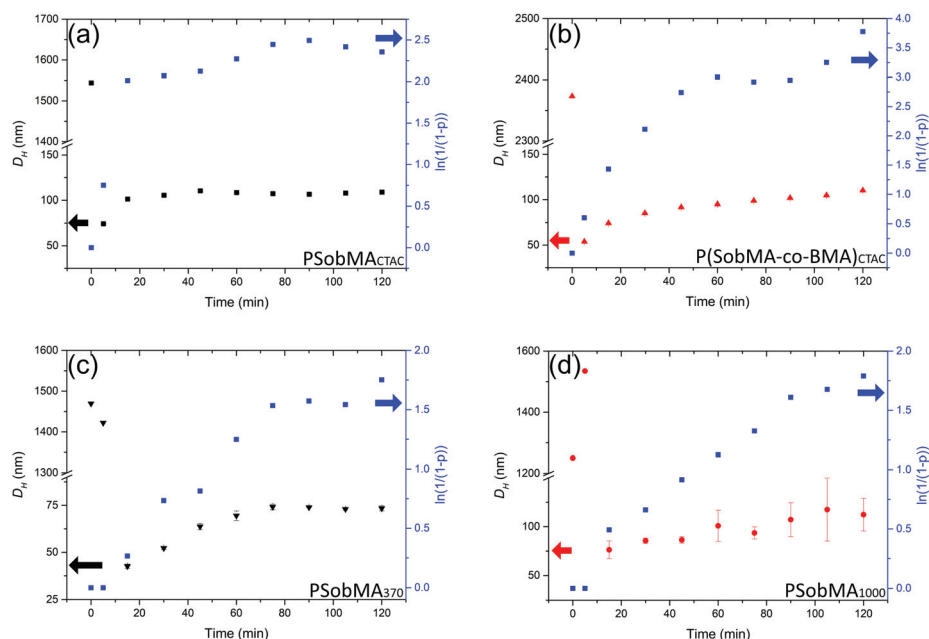

Fig. 3 The evolution of the hydrodynamic diameter (D_H) of the nanosized latexes prepared with surfactant-based emulsion polymerization (top line) and surfactant-free RAFT-mediated emulsion polymerization-induced self-assembly (PISA) (bottom line); (a) PSobMA$_{CTAC}$ (black squares), (b) P(SobMA-*co*-BMA)$_{CTAC}$ (red upward triangles), (c) PSobMA$_{370}$ (black downward triangles) and (d) PSobMA$_{1000}$ (red circles). In each graph the results are compared to the natural logarithm (ln(1/(1 − *p*)) of conversion (*p*) against reaction time (blue squares). In all graphs a break in the left *y*-axis was made for clarity. The error bars of D_H for the first two data points were removed for clarity.

higher reaction times, where all samples have reached a constant value listed in Table 1.

For PISA-latexes, the final size of the nanoparticles is sensitive to the initial ratio of monomer-to-macroRAFT which can be affected if monomers are evaporated during degassing (especially for small scale). Also, initiator efficiency plays a key role in both the conversion and particle size. For the emulsion polymerization, discrepancies can take place when the surfactant concentration is very close to or below the critical micelle concentration (CMC). Although in this work, the concentration of the surfactant was chosen to be almost two times higher than its CMC in order to avoid the aforementioned discrepancies.[33] Larger standard deviations are observed in stage C for the PSobMA$_{1000}$ which indicates batch-to-batch size variations. The difficulty to reach consistent final average size as the DP in the core grows too large, comparing the two PISA-latexes, seems specific to the SobMA monomer as it has not been shown in the same degree for MMA and BMA previously.[27] One can speculate that it is due to the stiffer character of the growing PSobMA chain in the core that might not allow for monomer diffusion as homogenously as for MMA/BMA systems, which is needed for the higher target DP to reach monodisperse results. Regardless of that, the diameter of PSobMA$_{1000}$ was found to be similar to that of the surfactant-based latex, i.e., 112 nm (Table 1).

An advantage of the RAFT-PISA process is the control of the final size of the latex by tuning the ratio between the hydrophobic and hydrophilic block, while using the same macroRAFT agent. Hence, the size and in extension the properties of the formed latexes can both be tailored. This was indeed the result of using the cationic PDMAEMA-based macroRAFT for the homopolymerization of SobMA in a surfactant-free PISA system. By comparing PSobMA$_{370}$ and PSobMA$_{1000}$ the particle diameter was increased by increasing the DP of the core, i.e. 73 and 112 nm, respectively (Table 1). In order to correlate the DLS data with the data obtained from ^{1}H-NMR, the kinetic plot (natural logarithm) is compared with the particle diameter (Fig. 3). The colloidal stability, which is governed by the cationic nature of the corona, as shown by ζ potential measurements, is maintained cationic at >+49 mV for all latexes (Table 1). Furthermore, the colloidal stability can be investigated by visual observations. None of the latexes exhibited phase separation or sedimentation during the experiments as well as after storage at 4 °C for approximately 8 months.

Morphological and thermal properties of nanolatexes

It is important to understand the differences between the wet and the dry state of a latex sample and, in extension, what effect that has on the final coating applications. Hence, in this part, the morphological properties in both states as well as their thermal properties will be discussed. The morphological characterization of dry samples was achieved by using atomic force microscopy (AFM) and field emission scanning electron microscopy (FE-SEM). The results obtained are further compared with the DLS results.

The latex samples were diluted (0.1 wt%) and spin coated on clean silica wafers and characterized by AFM (Fig. 4) and FE-SEM (Fig. S8†) without prior dialysis. Both microscopy techniques verified the spherical geometry of nanoparticles (Table 1). The size values obtained differ from those obtained by DLS, but they exhibit the same pattern. The differences in size we observed by comparing FE-SEM, AFM with DLS are due to two reasons: In DLS, the nanolatexes are in the wet state whereas in AFM and FE-SEM, in the dry state. When a latex sample is dried all water present in the core will evaporate, thus the size will be decreased. Furthermore, in DLS larger particles influence the final diameter more, due to the relation between the incident light and the particle size.[34–36] Additionally, the large standard deviations in the FE-SEM and AFM diameter (Table 1) are the result of using the whole area of the micrographs.

For the coating applications of latexes and in order to create a film of the nanolatexes onto cellulose, the knowledge of the film formation behaviour and the polymeric components glass transition temperature (T_g) is of utmost importance.[37] Therefore, their thermal properties were investigated by DSC (Table 1, Fig. S7†). It has been reported that PSobMA exhibit a rather high T_g, ranging from 116 to 155 °C, depending on both the polymerization technique and molecular weight used.[9] In this work, that observation is verified. All SobMA-based latexes reach high T_g values. Additionally, by increasing the molecular weight of SobMA, the T_g is also slightly increasing, i.e. 119 and 127 °C for PSobMA$_{370}$ and PSobMA$_{1000}$, respectively. However, considering the standard deviations, the T_g values are not significantly different. According to the Flory-Fox equation and assuming full miscibility of monomers, it is expected that the T_g will be decreased when SobMA is copolymerized with BMA.[38] The final T_g of P(SobMA-co-BMA)$_{CTAC}$ was found to be 50 °C, which is slightly
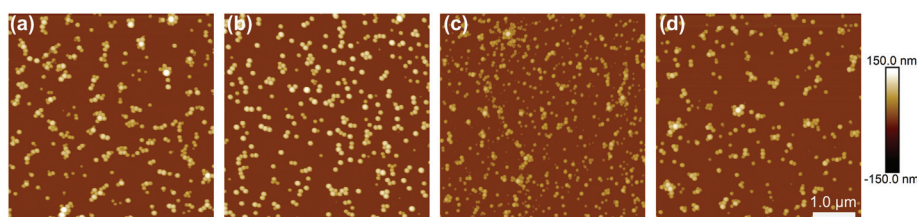

Fig. 4 AFM Imaging results of the investigated nanolatexes. (a) PSobMA$_{CTAC}$, (b) P(SobMA-co-BMA)$_{CTAC}$, (c) PSobMA$_{370}$ and (d) PSobMA$_{1000}$. The scale bar is 1 μm for all images.

higher than the theoretical value obtained from the Flory-Fox equation, *i.e.* 38 °C (eqn (S7)†). Similar discrepancies were also observed in a previous study.[9]

Adsorption of nanolatexes onto cellulose

The film formation properties of the nanolatexes are investigated and discussed in this part. Specifically, the ability of the nanolatexes to adsorb onto cellulose was investigated thoroughly with FE-SEM, where the morphological characteristics are studied. Additionally, with the formation of a film, the wetting is expected to change, thus, the contact angle (CA) against water was measured. Furthermore, the adsorption is compared with commercial sulfate polystyrene latex (PS latex), which are larger, anionically stabilized particles and exhibit a lower T_g (104 °C) than the latexes synthesized in this work (Table 1).

To investigate the film formation that the nanolatexes undergo on cellulose, pieces of cellulose (filter paper) were immersed in latex dispersion (1 wt%) for 24 h and either annealed above their T_g (150 °C) for 1 and 8 h or left to dry without annealing. In order to verify the successful adsorption, the filter papers were studied by FT-IR (Fig. S9†). It can be confirmed that the carbonyl peak at approximately 1730 cm^{-1} is present for all samples, which originates from the ester groups present in all investigated latex polymers.

In order to verify that the substrate remains unaffected by the heat treatment, the surface morphology of pristine cellulose was studied by FE-SEM (Fig. S10†). The unmodified cellulose samples were subjected to the same annealing protocol as the latex-modified samples, which showed no macroscopic

differences. Additionally, low magnification images of modified cellulose samples were also taken (Fig. S11†). The cellulose samples modified with the surfactant-based latexes were the only ones to show clear features of film formation after 8 h.

In order to highlight the morphological differences originating from the two different synthetic procedures, cellulose modified with PSobMA$_{CTAC}$ and PSobMA$_{370}$ were compared with samples modified with PS latex (Fig. 5). It can be observed that spherical particles occupy most of the untreated substrate, which indicates successful adsorption. For PSobMA$_{1000}$ (Fig. S12†) a range of differently sized nanolatexes is observed which can be directly correlated to the high standard deviation in the size values obtained by DLS (Table 1). When the latex samples are annealed a film is created, which is characterized by two stages; polymer interdiffusion and the final film formation.[39,40] In our case, after 1 h of annealing, the latexes start to coalesce and fuse together with their neighbouring nanoparticles through polymer interdiffusion (Fig. 5b, e and h). The coalescence is most efficient for the P(SobMA-*co*-BMA)$_{CTAC}$ (Fig. S12†) and PS latex samples, which exhibit clear features of film formation. The reason for that lies in the low T_g value of these samples compared with the high T_g latexes. When the samples were annealed for 8 h, all nanoparticles have coalesced and coherent films are formed. The copolymer modified cellulose sample did not exhibit any morphological differences after 8 h, which suggest that a thermally stable film is formed. Interestingly, for the PISA latexes it can be observed that even after 8 h of annealing there are locations where aggregates of uncoalesced nanoparticles are apparent. The
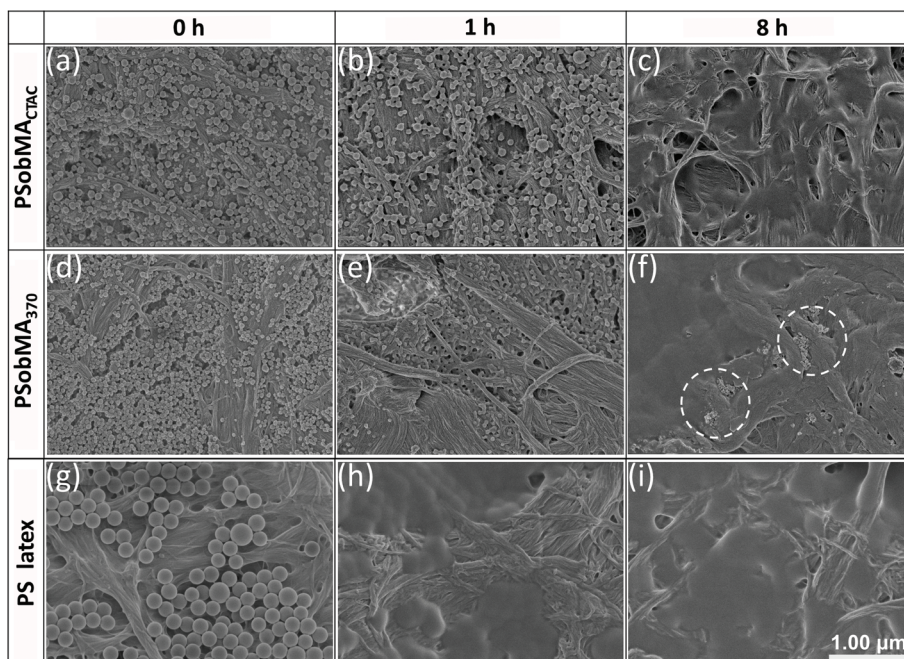

Fig. 5 FE–SEM images of cellulose filter paper on top of which nanolatexes are adsorbed; (a–c) PSobMA$_{CTAC}$, (d–f) PSobMA$_{370}$ and (g–i) PS latex. Additionally, each sample was subjected to annealing at 150 °C for different amount of time; (a, d and g) before annealing, (b, e and h) 1 h of annealing and (c, f and i) 8 h of annealing. The magnification is ×35 k and the scale bar is 1 µm for all images.

Table 2 Contact angle (CA) values of the modified cellulose filter papers at different annealing times at 150 °C. Each value is an average of at least five measurements

Samples	CA (°)		
	0 h	1 h	8 h
PSobMA$_{CTAC}$	30 ± 9	78 ± 20	85 ± 13
P(SobMA-co-BMA)$_{CTAC}$	90 ± 11	104 ± 4	106 ± 13
PSobMA$_{370}$	29 ± 9	67 ± 20	63 ± 13
PSobMA$_{1000}$	33 ± 8	101 ± 23	70 ± 15
PS latex	16 ± 2	63 ± 10	86 ± 9

observed thermal stability seems to be an effect of the structural stability imposed by the charged corona, corroborating previous studies of PISA-latexes in which very high colloidal stability was observed in the wet state but also to some degree in dried state where tougher annealing was needed to disrupt and fuse the nanoparticle boundaries, despite a low T_g core polymer.[28,40]

An alternative and indirect way to study the film formation on cellulose is by monitoring the difference in wetting before and after annealing. For the case of non-modified cellulose, the CA could not be assessed due to the instant absorption of the water droplet, confirming the hydrophilic nature of the substrate. Consequently, the formation of a polymer coating with hydrophobic units is expected to result in increased hydrophobicity. In order to study this, the CAs against water were measured (Table 2). The CA for all modified samples increases after 1 h and 8 h of annealing, respectively, where the highest value recorded belongs to P(SobMA-co-BMA)$_{CTAC}$ (106°). In Table 2 it can be observed that P(SobMA-co-BMA)$_{CTAC}$-modified cellulose sample exhibits a high CA value even before annealing, which can be explained by the fact that a partial polymeric film was created even before the annealing, due to the low T_g of the nanolatex (Fig. S13†). However, all of the PISA-modified samples exhibited lower CA values when compared with similar systems where PMMA and PBMA were used as the hydrophobic core.[27]

Conclusions

In this work, bio-based cationic nanolatexes, comprised of SobMA, a derivative of the terpene α-pinene, were successfully synthesized with and without surfactant. In the former case, nanolatexes stabilized by the cationic surfactant CTAC were produced by employing emulsion polymerization. In the latter case, RAFT-mediated emulsion polymerization with PISA was employed and the nanolatexes were stabilized by the cationic macroRAFT agent comprised of P(DMAEMA-co-MAA). Both cases yielded spherical nanosized latexes with diameters ranging between 70 and 110 nm, according to DLS, the geometry of which was further verified with AFM and FE-SEM. The kinetic profile of these nanolatexes highlighted the differences between the two polymerization techniques. Thereafter, they were adsorbed on cellulose (filter paper) and annealed at

150 °C for different amounts of time. The annealing resulted in the creation of a polymer coating on top of the cellulose substrate which exhibited a hydrophobic character according to CA. Finally, the film formation mechanism was studied by FE-SEM and gave a better understanding on how the investigated nanolatexes were fused together to yield the polymeric film, also indicating that PISA-nanolatexes are more thermally stable and resist coalescence to larger degree than the conventional CTAC-based latexes.

Conflicts of interest

There are no conflicts to declare.

Acknowledgements

Notes and references

1 R. Lambourne and T. A. Strivens, *Paint and surface coatings: theory and practice*, 1999.
2 B. Yamada and P. B. Zetterlund, *Handbook of Radical polymerization*, 2002, pp. 117–186.
3 G. Odian, *Emulsion Polymerization*, 2004, pp. 350–371.
4 F. H. Isikgor and C. R. Becer, *Polym. Chem.*, 2015, **6**(25), 4497–4559.
5 F. L. Hatton, *Polym. Chem.*, 2020, **11**(2), 220–229.
6 Y. Zhu, C. Romain and C. K. Williams, Sustainable polymers from renewable resources, *Nature*, 2016, **540**, 354–362.
7 A. Gandini and T. M. Lacerda, *Prog. Polym. Sci.*, 2015, **48**, 1–39.
8 M. S. Lima, C. S. M. F. Costa, J. F. J. Coelho, A. C. Fonseca and A. C. Serra, *Green Chem.*, 2018, **20**(21), 4880–4890.
9 A. Stamm, M. Tengdelius, B. Schmidt, J. Engström, P. O. Syrén, L. Fogelström and E. Malmström, *Green Chem.*, 2019, **21**(10), 2720–2731.
10 J. T. P. Derksen, F. P. Cuperus and P. Kolster, *Ind. Crops Prod.*, 1995, **3**(4), 225–236.
11 M. Moreno, M. Goikoetxea, J. C. de la Cal and M. J. Barandiaran, *Polym. Chem.*, 2014, **52**(24), 3543–3549.
12 G. Lligadas, J. C. Ronda, M. Galia and V. Cadiz, *Mater. Today*, 2013, **16**(9), 337–343.
13 J. Qui, B. Charleux and K. Matyajaszewski, *Prog. Polym. Sci.*, 2001, **26**(10), 2083–2134.

14 F. Ozer, M. O. Beskardes and E. Piskin, *J. Appl. Polym. Sci.*, 2000, **78**(3), 569–575.

15 S. A. F. Bon, M. Bosveld, B. Klumperman and A. L. German, *Macromolecules*, 1997, **30**(2), 324–326.

16 H. A. S. Schoonbrood and J. M. Asua, *Macromolecules*, 1997, **30**(20), 6034–6041.

17 S. C. Thickett and R. G. Gilbert, *Polymer*, 2007, **48**(24), 6965–6991.

18 P. B. Zetterlund, S. C. Thickett, S. Perrier, E. Bourgeat-Lami and M. Lansalot, *Chem. Rev.*, 2015, **115**(18), 9745–9800.

19 M. F. Cunningham, *Prog. Polym. Sci.*, 2002, **27**(6), 1039–1067.

20 C. J. Ferguson, *Macromolecules*, 2005, **38**(6), 2191–2204.

21 A. M. dos Santos, J. Pohn, M. Lansalot and F. D'Agosto, *Macromol. Rapid Commun.*, 2007, **28**(12), 1325–1332.

22 I. Chaduc, W. J. Zhang, J. Rieger, M. Lansalot, F. D'Agosto and B. Charleux, *Macromol. Rapid Commun.*, 2011, **32**(16), 1270–1276.

23 M. Lansalot, J. Rieger and F. D'Agosto, *Macromolecular Self-Assembly*, 2016, pp. 33–82.

24 F. L. Hatton, M. Ruda, M. Lansalot, F. D'Agosto, E. Malmström and A. Carlmark, *Biomacromolecules*, 2016, **17**(4), 1414–1424.

25 V. Ladmiral, A. Charlot, M. Semsarilar and S. P. Armes, *Polym. Chem.*, 2015, **6**(10), 1805–1816.

26 L. Carlsson, A. Fall, I. Chaduc, L. Wågberg, B. Charleux, E. Malmström, F. D'Agosto, M. Lansalot and A. Carlmark, *Polym. Chem.*, 2014, **5**(20), 6076–6086.

27 J. Engström, F. L. Hatton, L. Wågberg, F. D'Agosto, M. Lansalot, E. Malmström and A. Carlmark, *Polym. Chem.*, 2017, **8**(6), 1061–1073.

28 J. Engström, T. Benselfelt, L. Wågberg, F. D'Agosto, M. Lansalot, A. Carlmark and E. Malmström, *Nanoscale*, 2019, **11**, 4287–4302.

29 S. H. Thang, Y. K. Chong, R. T. A. Mayadunne, G. Moad and E. Rizzardo, *Tetrahedron Lett.*, 1999, **40**(12), 2435–2438.

30 G. Bouhadir, N. Legrand, B. Quiclet-Sire and S. Z. Zard, *Tetrahedron Lett.*, 1999, **40**(2), 277–280.

31 W. J. Zhang, F. D'Agosto, O. Boyron, J. Rieger and B. Charleux, *Macromolecules*, 2011, **44**(19), 7584–7593.

32 I. Chaduc, E. Reynaud, L. Dumas, L. Albertin, F. D'Agosto and M. Lansalot, *Polymer*, 2016, **106**, 218–228.

33 C. H. Tan, Z. J. Huang and X. G. Huang, *Anal. Biochem.*, 2010, **401**(1), 144–147.

34 C. M. Hoo, N. Starostin, P. West and M. L. Mecartney, *J. Nanopart. Res.*, 2008, **10**, 89–96.

35 P. Rademeyer, D. Carugo, J. Y. Lee and E. Stride, *Lab Chip*, 2105, **15**(2), 417–428.

36 S. Bhattacharjee, *J. Controlled Release*, 2016, **235**, 337–351.

37 J. Engström, C. J. Brett, V. Körstgens, P. Müller-Buschbaum, W. Ohm, E. Malmström and S. V. Roth, *Adv. Funct. Mater.*, 2020, **30**, 1907720.

38 T. G. Fox Jr. and P. J. Flory, *J. Appl. Phys.*, 1950, **21**(6), 581–591.

39 H. Kast, *Die Makromol. Chem.*, 1985, **10**(S19851), 447–461.

40 J. L. Keddie and F. Routh, *Fundamentals of latex film formation*, 2010.